Nonlinear Dynamics of Coupled Axion-Josephson Junction Systems

Jin Yan[a], Christian Beck[a]

[a]*School of Mathematical Sciences, Queen Mary University of London, Mile End Road, London E1 4NS, UK*

Abstract

We study the classical dynamics of an axion field (the signal) that is coupling into a Josephson junction (the detector) by means of a capacitive coupling of arbitrary size. Depending on the size of the coupling constant and the initial conditions, we find a rich phase space structure of this nonlinear problem. We present general analytic solutions of the equations of motion in the limit of small amplitudes of the angle variables, and discuss both the case of no dissipation and the case of dissipation in the system. The effect of a magnetic field is investigated as well, leading to topological phase transitions in the phase space structure.

Keywords: nonlinear dynamical systems, coupled Josephson junctions, axions, phase space analysis

1. Introduction

Axions are exotic particles that are predicted in many extensions of the standard model of elementary particle physics [1, 2, 3, 4, 5, 6, 7, 8, 9, 10, 11, 12]. The QCD axion is one of the main candidates for dark matter in the universe. The equations of motion of axions are very similar to those of Josephson junctions. This analogy has been discussed in detail in [9, 10, 11, 12] and possible detection schemes for axions or axion-like particles have been proposed based on this analogy, using Josephson junctions [13] as detectors, and assuming the possibility of a synchronisation between the axion and Josephson phase angle.

In this paper we are interested in the general behaviour of the classical nonlinear field equations that decribe this problem. We will study systematically the nonlinear dynamics aspects of this coupled initial value problem, i.e. a classical axion field that is coupled into a Josephson junction in a capacitive way, meaning the interaction strength is proportional to $c(\ddot{\varphi} - \ddot{\theta})$, where φ is the Josephson phase difference and θ the axion misalignment angle, c is the coupling constant. We keep the size of the coupling constant c as an arbitrary parameter and will study both very small, intermediate, and large values of c. Mathematically, the problem is equivalent to two coupled Josephson junctions, one with phase angle φ and the other one with phase angle θ. Surprisingly, a very rich and complex phase space structure arises as a function of the coupling, the frequency ratio and the initial conditions, which

we will describe in detail in the following sections. For previous work related to coupled Josephson junction-like systems, see e.g., [14, 15, 16, 17].

For small elongations of the angle variables and velocities, the problem becomes linear and describes two coupled harmonic oscillators. Of course this linear case is exactly solvable, and we will compare in our paper carefully the nonlinear effects due to the cosine potentials of the axion and junction as compared to the case of coupled harmonic oscillators with just a quadratic potential. We will deal with our coupled system in a general mathematical way, allowing in principle for arbitrary parameter combinations and analysing the classical phase space structure of this nontrivially coupled nonlinear system. It should be clear that this system has many different applications in physics: it describes not only the possible coupling of axions into a Josephson environment, but also the coupling of two classical q-bits [18, 19], which are coupled with a capacity, of relevance for nanotechnological applications. One can also think of two coupled pendulas that are coupled in a way that is proportional to the acceleration difference between the two pendulas, i.e. a classical mechanics problem with constraints in a constant gravitational field. Thus many generic physical interpretations are possible for the dynamical system that we systematically study in the following.

This paper is organized as follows:

In section 2 we study the phase space structure as a function of the coupling constant c, for suitable initial conditions that are physically motivated. Particular emphasis is put on coupling constants that are of the order $c \sim 10^{-3}$, which is a typical physically realized coupling strength in coupled q-bits [19]. In section 3 we focus on the dependence with respect to the ratio of Josephson junction frequency and axion frequency, emphasizing the sensitivity on this parameter, including resonance effects. In section 4 we study the dependence on initial conditions, in particular how the phase diagram changes when the initial $\dot{\varphi}(0)$ of the measuring Josephson junction is varied (in experiments, this can be easily achieved by varying the applied bias voltage). In section 5 we present analytic solutions of the general initial value problem in the limit case of small amplitudes and small angular velocities, where the problem reduces to two coupled (in a capacitive way) harmonic oscillators. In this section we will deal with arbitrary coupling strengths, without and with dissipation. The effect of an external magnetic field is discussed in section 6. Finally, our concluding remarks are given in section 7.

2. Nontrivial phase space structure as a function of the coupling strength c

We start by introducing the classical equations of motion of axions coupled into a Josephson junction environment. As worked out in [9], the coupled system of equations is given by

$$\ddot{\varphi} + a_1\dot{\varphi} + b_1\sin\varphi = c(\ddot{\theta} - \ddot{\varphi}) \tag{1a}$$

$$\ddot{\theta} + a_2\dot{\theta} + b_2\sin\theta = c(\ddot{\varphi} - \ddot{\theta}) \tag{1b}$$

where $\varphi(t)$ and $\theta(t)$ are the phase angle variables for the Josephson junction and axion, respectively. The parameters in the above equations, namely, the dissipation coefficients

(a_1, a_2) , the frequency parameters (b_1, b_2), and the coupling constant c depend on details of the physical model considered. For the measuring Josephson junction, $b_1 = \omega^2$ corresponds to the plasma frequency ω of the junction, and a_1 is given by $a_1 = 1/RC$, where R is the shunt resistance and C the capacity. For dark matter axions, the corresponding (a_2, b_2) parameters as well as the coupling strength c are unknown, although some conjectures have been formulated [9, 10, 11, 12] and some new experiments search in the relevant parameter region[20, 21, 22]. b_2 is given by the square of the axion mass. In the early universe one has $a_2 = 3H$ where H is the Hubble constant. At current times, $a_2 = 0$ in very good approximation. To the best of our knowledge, a detailed and systematic investigation of the mathematical properties of the system (1) as a function of the parameters is lacking, but this is higly relevant for future experimental axion searches that use Josephson junctions or coupled arrays of Josephson junctions as possible novel types of axion detectors [10, 11, 12]. Hence, in the following we explore the mathematical properties of the coupled system in more detail.

For simplicity, consider first the case with no dissipation ($a_1 = a_2 = 0$). Due to its nonlinearity, the system exhibits complex behavior as a function of the parameters, which in the following is investigated numerically by writing (1) as a system of four first-order differential equations and using the fourth-order Runge-Kutta method. Apart from the three parameters b_1, b_2 and c, the four initial conditions $(\varphi, \dot{\varphi}, \theta, \dot{\theta})_{t=0}$ are to be specified.

To study how the size of coupling constant c affects the behaviour of the system we fix $b_1 = b_2 = 1$ and vary c from 10^{-6} to 1. The initial conditions are chosen to be $(\varphi, \dot{\varphi}, \theta, \dot{\theta})_{t=0} = (0, 2, 0, 0)$ such that, in the absence of the axion, the Josephson junction would behave like a pendulum in a gravitational field just reaching the highest unstable point with zero momentum. The angular velocity of the axion is assumed to be small, and put equal to zero in our simulations in the following.

Figure 1 shows some phase space trajectories of the axion for small values of the coupling parameter c. The phase space portraits for the axion undergo a bifurcation-like process which we may call an *eversion process*[1]. This happens, for example, when we vary c from 2×10^{-6} to 6×10^{-6} (see figs.1a, 1b and 1c). A similar process also happens when c varies in the region $c = 1 \times 10^{-3} \sim 4 \times 10^{-3}$ (figs.1d, 1e and 1f): a 'pretzel-shaped' trajectory is deformed into a simple 'cardioid' and then becomes an 'inside-out pretzel'. As the phase φ of the Josephson junction is unbounded (i.e., φ is monotonically increasing with time), the whole four-dimensional phase trajectory is projected onto the $(\dot{\varphi}, \theta, \dot{\theta})$-subspace to illustrate the relation among the three bounded variables, see the last row in fig.1. The cusp appearing in fig.1h (or 1e) corresponds to the largest angular velocity of the Josephson junction, at which max $\dot{\varphi} = \dot{\varphi}(0) = 2$. The eversion occurs again at $c = 0.74 \sim 0.84$ (fig.2), but the cusp in fig.2b does not correspond to max $\dot{\varphi}$: the Josephson junction gains energy from the axion via a medium coupling so that the largest angular velocity exceeds the initial one.

---

[1]The word *eversion* means 'turning inside out', which is borrowed from differential topology. If we regard the trajectory as a curve lying on the surface of some three-dimensional manifold, then by varying the parameter the inside of the surface is turned outside smoothly and continuously.
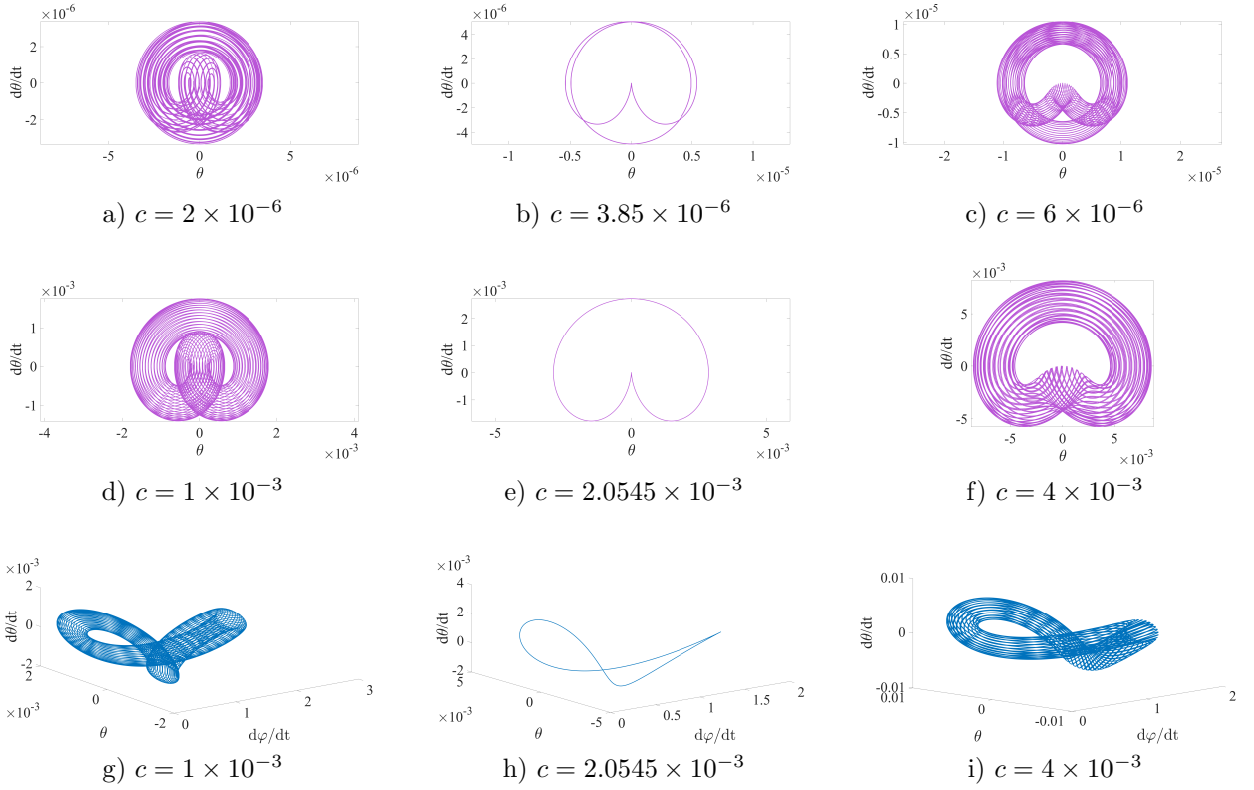
Figure 1: Eversion processes of the axion trajectory for weak couplings: upper two rows: axion phase portraits in the $(\theta, \dot{\theta})$-plane; last row: the corresponding $(\dot{\varphi}, \theta, \dot{\theta})$-subspace ($t_{max} = 500$)
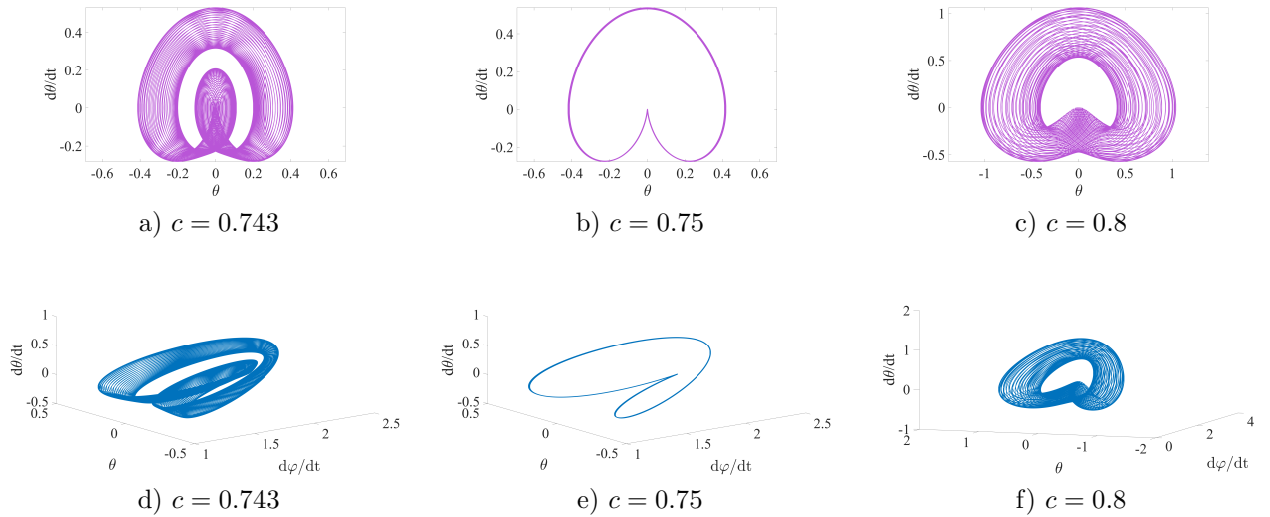

Figure 2: Same as Fig.1 but for medium couplings: upper row: axion phase portraits in the $(\theta, \dot{\theta})$-plane; lower row: the corresponding $(\dot{\varphi}, \theta, \dot{\theta})$-subspace ($t_{max} = 500$)

4

3. Dependence on the frequency ratio

As already mentioned, future detectors for galactic axions passing through the Earth may be based on Josephson junctions or arrays of Josephson junctions [10, 11, 12, 21] and in such a setting one expects resonance effects if the axion mass coincides with the plasma frequency of the junctions. Recall that the two parameters b_1 and b_2 are given by the square of the plasma frequency of the Josephson junction and the mass of the axion, respectively, and as outlined in [9] these parameters have similar order of magnitude. At a resonance point one has $b_1/b_2 = 1$, but we now want to explore what happens if the ratio is just close to 1.

We are interested in the dependence on the frequency ratio b_1/b_2 for the non-dissipative $(a_1 = a_2 = 0)$ case. In the following numerical experiment we fix the coupling $c = 2.0545 \times 10^{-3}$ (a 'cardioid' for $b_1 = b_2 = 1$) and, since the initial conditions are chosen to be $(\varphi, \dot{\varphi}, \theta, \dot{\theta})_{t=0} = (0, 2, 0, 0)$, we expect that the parameter b_1 has a stronger influence on the system than b_2 does. In addition, b_1 characterises the frequency of the Josephson junction, which can be easily adjusted in experiments; so we set $b_2 = 1$ and let b_1 slightly deviate from b_2, which experimentally corresponds to searching for an axion mass resonance in a given vicinity of the plasma frequency.

Figure 3 shows some phase space trajectories for different values of the frequency ratio. The first row shows the phase portraits of the axion for $b_1 = 1/0.9979, 1/0.9978$ and $1/0.9975$, respectively. As in this case all the four variables are bounded, we plot in the second and the third rows the projections onto the $(\dot{\varphi}, \theta, \dot{\theta})$-subspace and the $(\varphi, \theta, \dot{\theta})$-subspace, which respectively show the axion dynamics in relation to the angular velocity and the angle of the Josephson junction. In addition, the fourth variable, $\dot{\varphi}$, is indicated by color in the last two rows of the figure.
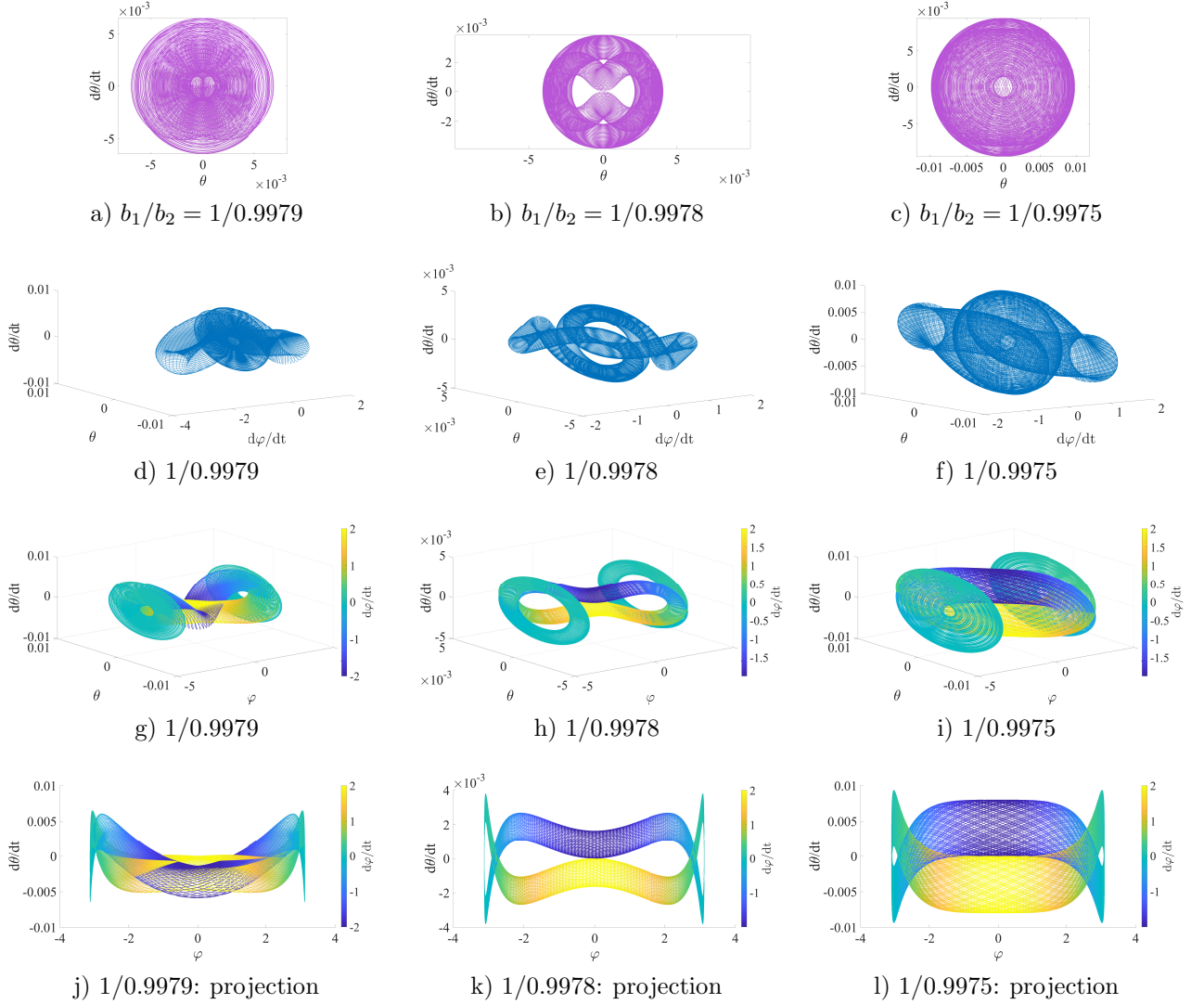
Figure 3: Frequency ratio dependence: First row: the axion phase portraits in the $(\theta, \dot{\theta})$-plane; second row: the $(\dot{\varphi}, \theta, \dot{\theta})$-subspace; third row: the $(\varphi, \theta, \dot{\theta})$-subspace with color coding $\dot{\varphi} \in [-2, 2]$; last row: the projection onto $(\varphi, \dot{\theta})$ with color coding $\dot{\varphi} \in [-2, 2]$ ($t_{max} = 2500$). One notices an extremely sensitive dependence on the ratio b_1/b_2.

Notice that the two cyan 'wheels' in the $(\varphi, \theta, \dot{\theta})$-subspace indicate that the angular velocity of the Josephson junction, $\dot{\varphi}$, is nearly zero, which corresponds to a large angle φ (unstable top stationary point of pendulum), but conditioned on this small velocity the axion's motion is nontrivial; the energy has been transformed from the Josephson junction to the axion so that it could oscillate with a relatively large amplitude. The dark blue and light yellow bands connecting these two 'wheels' are equivalent due to orientation symmetry of the rotation in the Josephson junction's phase ($\dot{\varphi} = -v$ for dark blue and $\dot{\varphi} = v$ for light yellow). As the ratio b_1/b_2 changes, the two bands can cross each other, indicating that whenever $\varphi \to 0$ with $\dot{\varphi} < 0$ the axion angular velocity is always negative ($\dot{\theta} < 0$), which

6

is the opposite to the case that the two bands do not cross - their oscillations always have opposite orientations: $\dot{\theta} > 0$ when $\dot{\varphi} < 0$. This might indicate a method in the experiment to determine the frequency ratio - by looking at the direction of the motion.

It is interesting to notice the extreme sensitivity with respect to the parameter b_1: in the case of $b_1 = b_2 = 1$ the phase variable of the Josephson junction increases monotonically, indicating that it undergoes circular motion; while for b_1 slightly larger than 1 (say, $1/0.9979 \leq b_1 \leq 1/0.9$) it oscillates between two angles, just like a pendulum cannot reach the highest point if the energy is not large enough to overcome the gravitational potential at the top. The phase trajectory in this case is just a simple 'eye-shaped' closed curve. The three-dimensional subspace projections of the whole four-dimensional phase portrait change nontrivially, but the deformation still resembles an eversion process, as seen in the previous section.

For the case that b_1 largely deviates from $b_2 = 1$ (for example $b_1 \sim 0.1$ or $b_1 \sim 2$) the topology of the phase trajectory does not change significantly under parameter changes.

4. Dependence on the initial angular velocity

4.1. No dissipation

There are only two degrees of freedom in the choices of initial conditions since we can always set the initial phases, $\varphi(0)$ and $\theta(0)$, to be zero by a simple coordinate transformation. In the absence of dissipation for both the Josephson junction and the axion ($a_1 = a_2 = 0$), for our numerical experiment we fix the weak coupling as $c = 2.0545 \times 10^{-3}$, set $b_1 = b_2 = 1$ and vary the initial angular velocity of the Josephson junction ($\dot{\varphi}(0)$) from 1 to 10, while keeping the axion's initial angular velocity small, say, $\dot{\theta}(0) = 0$. The initial angular velocity of the Josephson junction can be easily manipulated in experiments, by applying a constant voltage across the junction.

Interestingly, for $\dot{\varphi}(0) \approx 1.95$ we see another eversion process (first row in fig.4), which has not been observed in the previous sections. Note: for each of the three cases in the first row in fig.4 the phase portrait of the Josephson junction is just a standard 'eye-shaped' closed curve, while for the cases in the last row the phase variable of the Josephson junction is monotonically increasing because, in the mechanical analogue, it has enough energy to cross the top (unstable) point of the pendulum, it performs a circular motion and continues to do so.

Comparing the last row in the above plots with the second row in fig.1, increasing the initial angular velocity of the Josephson junction around 2 is somewhat equivalent to increasing the coupling around 2.0545×10^{-3} — both produce to a 'cardioid' deformation and an eversion phenomenon.
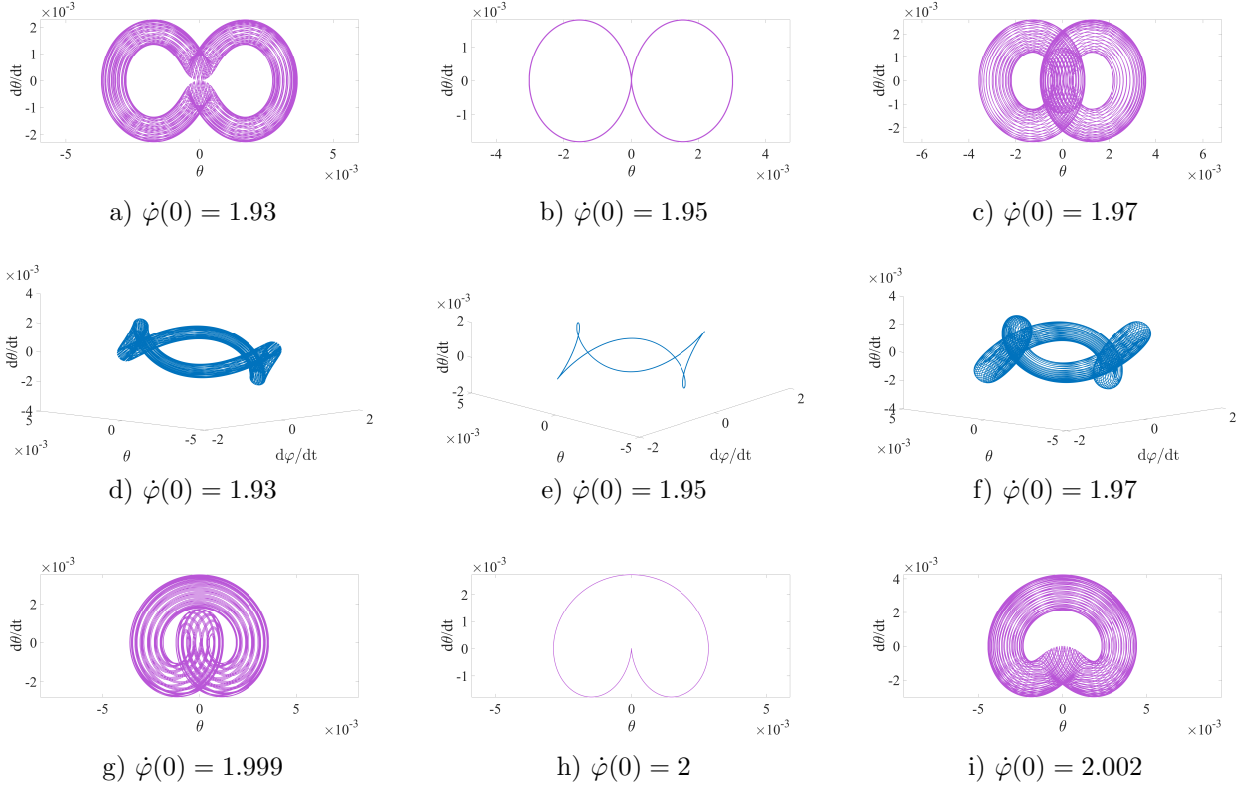
Figure 4: Initial angular velocity dependence: first and third rows: axion phase portraits in the $(\theta, \dot{\theta})$-plane; second row: the corresponding $(\dot{\varphi}, \theta, \dot{\theta})$-subspace ($t_{max} = 500$). Again an eversion process is visible, but this time as a function of the initial angular velocity $\dot{\varphi}(0)$.

Continuously increasing the initial angular velocity of the Josephson junction results in different patterns in the time series and in the phase portrait of the axion, see fig.5. Each time series has a high-frequency component that oscillates within a slowly varying profile, so the solution $\theta(t)$ can be approximated by a periodic (sinusoidal) function with a slowly varying amplitude.
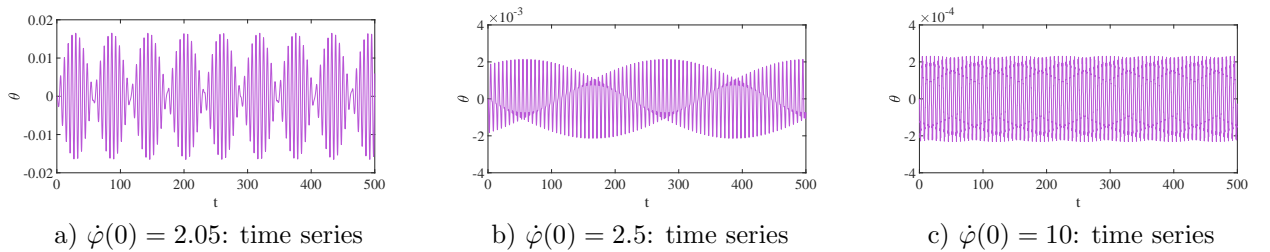

Figure 5: Initial angular velocity dependence: the axion time series $(t, \theta(t))$ ($t_{max} = 500$)

4.2. Dissipative system

For the dissipative case it is physically reasonable to assume that the damping coefficient of the axion, a_2, is small, so for simplicity we set $a_2 = 0$. By varying a_1 from 10^{-7} to 1 we found that the system approaches various limit cycles depending on the initial value of the axion angular velocity $\dot{\theta}(0)$, and the time for reaching a limit cycle depends on the value of a_1.

5. Analytic solutions in the limit of small oscillations

While many of the phenomena in the previous section are clearly produced by strong nonlinearities in the system dynamics, we now present some analytic results for small elongations. If the oscillation amplitudes of both Josephson junction and axion are small, then the original system (1) can be approximated as a linearised model, i.e. by the first-order approximation

$$\ddot{\varphi} = -a_1\dot{\varphi} - b_1\varphi + c(\ddot{\theta} - \ddot{\varphi}) \tag{2a}$$

$$\ddot{\theta} = -a_2\dot{\theta} - b_2\theta + c(\ddot{\varphi} - \ddot{\theta}) \tag{2b}$$

For simplicity we set $a_1 = a_2 = a > 0$, $b_1 = b_2 = 1$ and $c > 0$.

The system becomes uncoupled via the transformation $(\theta_+, \theta_-) = (\frac{1}{2}(\varphi + \theta), \frac{1}{2}(\varphi - \theta))$ and it reads in the new coordinates

$$\ddot{\theta}_+ = -a\dot{\theta}_+ - \theta_+ \tag{3a}$$

$$\ddot{\theta}_- = \frac{-a}{1+2c}\dot{\theta}_- - \frac{1}{1+2c}\theta_- \tag{3b}$$

Note that the above coordinate transformation decouples the system for arbitrary coupling strengths, including very large c. The general solutions in the new coordinates are then given by

$$\theta_+(t) = C_1 e^{\frac{1}{2}(-a-\sqrt{a^2-4})t} + C_2 e^{\frac{1}{2}(-a+\sqrt{a^2-4})t} \tag{4a}$$

$$\theta_-(t) = C_3 e^{\frac{1}{2}(-\alpha-\sqrt{\alpha^2-4\beta})t} + C_4 e^{\frac{1}{2}(-\alpha+\sqrt{\alpha^2-4\beta})t} \tag{4b}$$

where $\alpha = \frac{a}{1+2c}$ and $\beta = \frac{1}{1+2c}$, provided $a \neq 2$ and $\alpha^2 \neq 4\beta$. Otherwise,

1) if $a = 2$, the solution for θ_+ is

$$\theta_+(t) = C_1 e^{-t} + C_2 e^{-t}t \tag{5}$$

2) if $\alpha^2 = 4\beta$, or $a = 2\sqrt{1+2c}$, the solution for θ_- is

$$\theta_-(t) = C_3 e^{-\frac{1}{\sqrt{1+2c}}t} + C_4 e^{-\frac{1}{\sqrt{1+2c}}t}t \tag{6}$$

where the constant coefficients C_1, C_2, C_3 and C_4 are to be determined by the initial conditions $(\varphi, \dot{\varphi}, \theta, \dot{\theta})_{t=0}$, or equivalently $(\theta_+, \dot{\theta}_+, \theta_-, \dot{\theta}_-)_{t=0}$.

9

5.1. Non-dissipative case

In the case that $a = 0$ the solutions are simply given by

$$\theta_+(t) = C_1 \cos t + C_2 \sin t \tag{7a}$$

$$\theta_-(t) = C_3 \cos\left(\frac{1}{\sqrt{1+2c}}t\right) + C_4 \sin\left(\frac{1}{\sqrt{1+2c}}t\right) \tag{7b}$$

Imposing our example of initial conditions $(\varphi, \dot{\varphi}, \theta, \dot{\theta})_{t=0} = (0, 2, 0, 0)$, we get $C_1 = C_3 = 0$, $C_2 = 1$ and $C_4 = \sqrt{1+2c}$. Thus, the solutions in the original coordinates are given by

$$\varphi(t) = \theta_+ + \theta_- = \sin t + \sqrt{1+2c} \sin\left(\frac{1}{\sqrt{1+2c}}t\right) \tag{8a}$$

$$\theta(t) = \theta_+ - \theta_- = \sin t - \sqrt{1+2c} \sin\left(\frac{1}{\sqrt{1+2c}}t\right) \tag{8b}$$

Note that the solutions involve two frequencies, $\omega_+ = 1$ and $\omega_- = \frac{1}{\sqrt{1+2c}}$, which are commensurate if $\sqrt{1+2c}$ is rational. The phase trajectory is dense if the two frequencies are incommensurate.

An interesting result is concerned with possible synchronisation behavior of the two coupled oscillators. We found that, for some values of the coupling c (of measure zero on $\mathbb{R}$), the phase trajectories of φ and θ are identical up to a time translation. A simple proof of this result is provided here:

We set the initial conditions as $(\varphi, \dot{\varphi}, \theta, \dot{\theta})_{t=0} = (0, v_1, 0, v_2)$. Then by eqns.(7) the constants C_1 and C_3 are always zero; hence we get solutions $\varphi(t)$ and $\theta(t)$ which are combinations of two sine functions:

$$\varphi(t) = \theta_{+0} \sin t + \frac{1}{\omega_-}\theta_{-0} \sin\omega_- t \tag{9a}$$

$$\theta(t) = \theta_{+0} \sin t + \frac{1}{\omega_-}\theta_{-0} \sin\omega_- t \tag{9b}$$

where $\omega_- = \frac{1}{\sqrt{1+2c}}$, with $\theta_{+0} = \frac{\dot{\varphi}(0)+\dot{\theta}(0)}{2} = \frac{v_1+v_2}{2}$ and $\theta_{-0} = \frac{\dot{\varphi}(0)-\dot{\theta}(0)}{2} = \frac{v_1-v_2}{2}$.
With $y_i = \dot{x}_i$ ($i = 1, 2$) the parametrised trajectories in each phase plane are written as

$$x_1(t_1) = \theta_{+0} \sin t_1 + \frac{1}{\omega_-}\theta_{-0} \sin\omega_- t_1 \tag{10a}$$

$$y_1(t_1) = \theta_{+0} \cos t_1 + \theta_{-0} \cos\omega_- t_1 \tag{10b}$$

$$x_2(t_2) = \theta_{+0} \sin t_2 - \frac{1}{\omega_-}\theta_{-0} \sin\omega_- t_2 \tag{11a}$$

$$y_2(t_2) = \theta_{+0} \cos t_2 - \theta_{-0} \cos\omega_- t_2 \tag{11b}$$

10

Denote the differences by

$$\Delta x = x_1 - x_2 = \theta_{+0}(\sin t_1 - \sin t_2) + \frac{1}{\omega_-}\theta_{-0}(\sin \omega_- t_1 + \sin \omega_- t_2) \tag{12a}$$

$$\Delta y = y_1 - y_2 = \theta_{+0}(\cos t_1 - \cos t_2) + \theta_{-0}(\cos \omega_- t_1 + \cos \omega_- t_2) \tag{12b}$$

or

$$\Delta x = 2\theta_{+0}\cos\frac{t_1+t_2}{2}\sin\frac{t_1-t_2}{2} + \frac{2}{\omega_-}\theta_{-0}\cos\frac{\omega_-(t_1-t_2)}{2}\sin\frac{\omega_-(t_1+t_2)}{2} \tag{13a}$$

$$\Delta y = -2\theta_{+0}\sin\frac{t_1+t_2}{2}\sin\frac{t_1-t_2}{2} + 2\theta_{-0}\cos\frac{\omega_-(t_1+t_2)}{2}\cos\frac{\omega_-(t_1-t_2)}{2} \tag{13b}$$

By performing a linear transformation

$$t_1 = t + \tau \tag{14a}$$

$$t_2 = t \tag{14b}$$

the above differences become

$$\Delta x = 2\theta_{+0}\cos\frac{2t+\tau}{2}\sin\frac{\tau}{2} + \frac{2}{\omega_-}\theta_{-0}\cos\frac{\omega_-\tau}{2}\sin\frac{\omega_-(2t+\tau)}{2} \tag{15a}$$

$$\Delta y = -2\theta_{+0}\sin\frac{2t+\tau}{2}\sin\frac{\tau}{2} + 2\theta_{-0}\cos\frac{\omega_-(2t+\tau)}{2}\cos\frac{\omega_-\tau}{2} \tag{15b}$$

The differences are identically zero for all t and all initial velocities if we set

$$\sin\frac{\tau}{2} = 0 \tag{16a}$$

$$\cos\frac{\omega_-\tau}{2} = 0 \tag{16b}$$

or equivalently,

$$\tau = 0 \quad \mod 2\pi \tag{17a}$$

$$\omega_-\tau = \pi \quad \mod 2\pi \tag{17b}$$

If $\omega_- = \frac{p}{q}$ rational with $\gcd(p,q) = 1$, this can be written as $\omega_- = \frac{2k_1+1}{2k_2}$ $(k_1, k_2 \in \mathbb{N})$, and if we write $\tau = 2k\pi$ $(k \in \mathbb{N})$, then the above conditions are satisfied

$$\frac{2k_1+1}{2k_2}2k\pi = \pi \quad \mod 2\pi$$

provided $k = k_2$.

In conclusion, the phase trajectories for the non-dissipative linearised system (2) are identical[2] if $\omega_- := \frac{1}{\sqrt{1+2c}} = \frac{2k_1+1}{2k}$, or equivalently, $c = \frac{2k^2}{(2k_1+1)^2} - \frac{1}{2}$ with $k, k_1 \in \mathbb{N}$, and the

---

[2]'Identical' in the strict sense that the two trajectories must be closed, i.e., the two frequencies are commensurate, which is guaranteed by setting ω_- rational. One can also define what 'identical' (in a loose way) means for two open trajectories which not necessarily requires ω_- to be rational.

time series of the two phase variables are shifted by time $\tau = 2k\pi$. These values of c form a subset of the set of rational numbers in $\mathbb{R}$, which is obviously of measure zero.

Let us illustrate these general results with some examples: When $\omega_- = \frac{19}{8}$ (or $c = -\frac{297}{722}$), $\omega_- = \frac{1}{6}$ (or $c = \frac{35}{2}$) and $\omega_- = \frac{3}{4}$ (or $c = \frac{7}{18}$), the two identical trajectories are shown in fig.6 in row 1, 2, and 3, respectively.
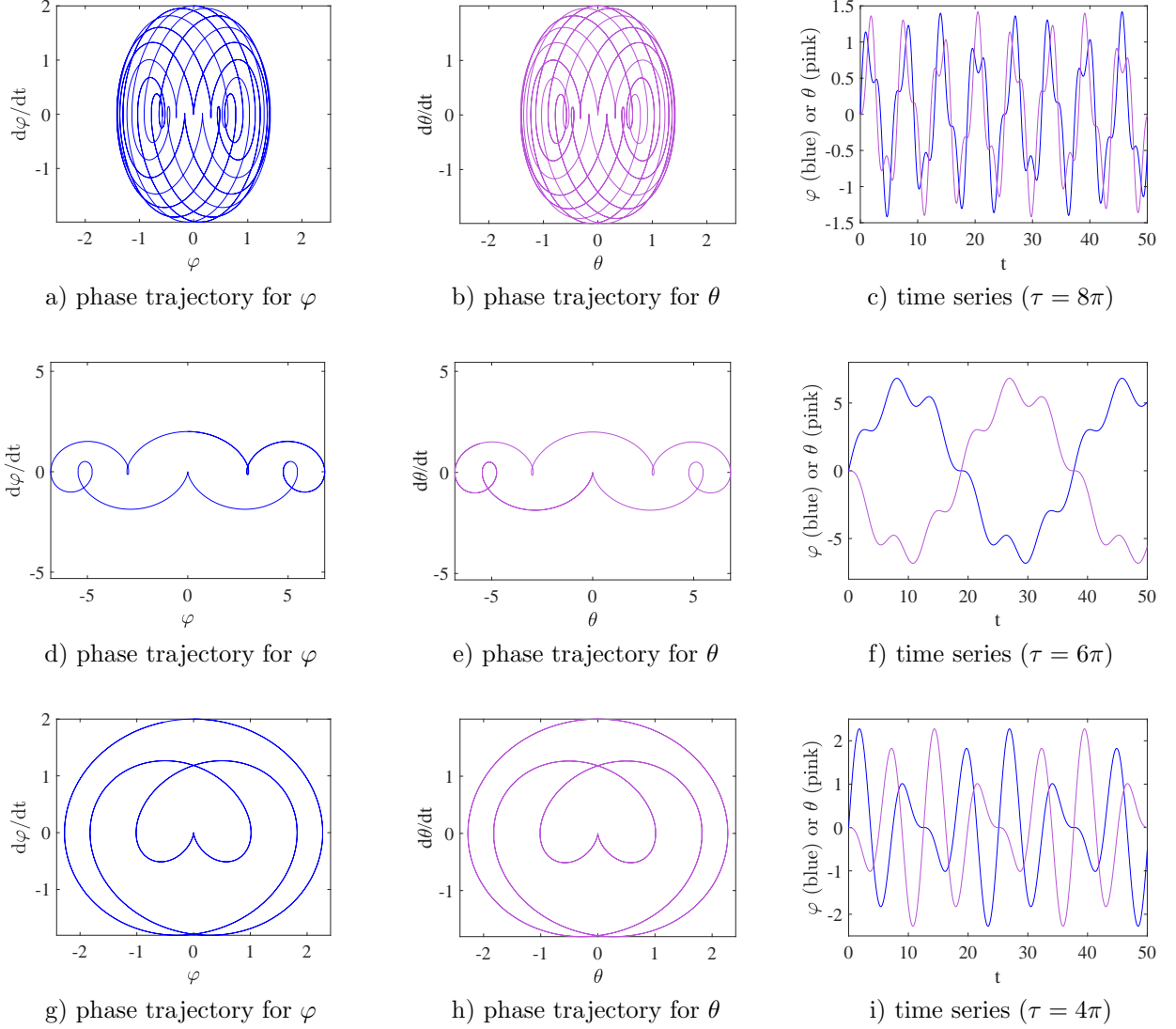

Figure 6: Examples of identical trajectories: by time shifting by τ in each case the two solution curves are identical ($t_{max} = 50$). First row: $\omega_- = \frac{19}{8}$ (or $c = -\frac{297}{722}$); second row: $\omega_- = \frac{1}{6}$ (or $c = \frac{35}{2}$); third row: $\omega_- = \frac{3}{4}$ (or $c = \frac{7}{18}$). Still a highly nontrivial phase portrait arises in the phase space, which depends on the integers k, k_1 that make up the coupling c.

Notice that if $k \approx k_1 \to \infty$, then $c \to 0$ (very weak coupling), $\omega_- \to 1 = \omega_+$, and the two trajectories will be identical although it requires a long time shift, $\tau \to \infty$, for their

solution curves to coincide. On the other hand, for the solutions (9) the period p given by $p = \gcd(p_1, p_2) = \gcd(\frac{2\pi}{\omega_+}, \frac{2\pi}{\omega_-}) = \gcd(2\pi, 2\pi \cdot \frac{2k}{2k_1+1}) = 2\pi \cdot \gcd(1, \frac{2k}{2k_1+1}) = 2\pi(2k_1 + 1) \to \infty$.

In particular, for different relations between k_1 and k the asymptotic trajectory follows different patterns. For example, the last row in fig.6 has a heart-shaped pattern in the centre, for which $(k_1, k) = (k_1, k_1 + 1) = (1, 2)$. As k_1 increases, the coupling parameter c decreases to zero from above, and the winding number (with respect to the origin of the phase plane) increases, see fig.7 below. Inspired by the first and second rows in fig.6, one can also choose some other relations between the two integers (k_1, k) to get different sequences of trajectories and eventually obtain a different asymptotic structure.
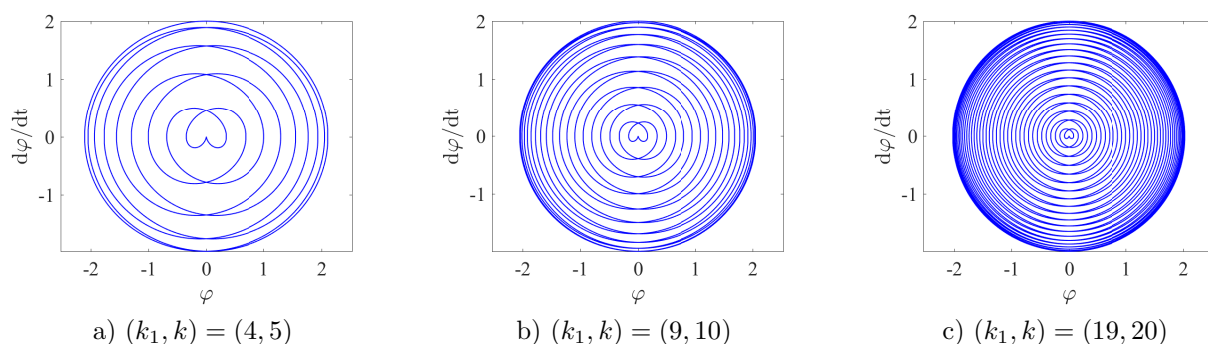

a) $(k_1, k) = (4, 5)$ b) $(k_1, k) = (9, 10)$ c) $(k_1, k) = (19, 20)$

Figure 7: An example of trajectory patterns for $k = k_1 + 1$ as $k_1 \in \mathbb{R}_+$ increases. Phase trajectories for φ (and also for θ as they are identical) are shown.

5.2. Dissipative cases

If $a \neq 0$, the two critical values of a divide the solutions into the following five categories: $(c > 0)$

(i) $0 < a < 2$ (small dissipation):

$$\varphi(t) = \frac{2}{\sqrt{4 - a^2}} e^{-\frac{a}{2}t} \sin\left(\frac{\sqrt{4 - a^2}}{2} t\right) + \frac{2}{\sqrt{4\beta - \alpha^2}} e^{-\frac{\alpha}{2}t} \sin\left(\frac{\sqrt{4\beta - \alpha^2}}{2} t\right) \tag{18a}$$

$$\theta(t) = \frac{2}{\sqrt{4 - a^2}} e^{-\frac{a}{2}t} \sin\left(\frac{\sqrt{4 - a^2}}{2} t\right) - \frac{2}{\sqrt{4\beta - \alpha^2}} e^{-\frac{\alpha}{2}t} \sin\left(\frac{\sqrt{4\beta - \alpha^2}}{2} t\right) \tag{18b}$$

where $\alpha = \frac{a}{1+2c}$ and $\beta = \frac{1}{1+2c}$. Because of the presence of small dissipation, both phase variables exhibits oscillatory decay, with two frequencies $(\omega_+, \omega_-) = (\frac{\sqrt{4-a^2}}{2}, \frac{\sqrt{4\beta - \alpha^2}}{2}) = (\frac{\sqrt{4-a^2}}{2}, \frac{\sqrt{4(1+2c)-a^2}}{2(1+2c)})$ and two decaying rates $(\nu_+, \nu_-) = (\frac{a}{2}, \frac{\alpha}{2}) = (\frac{a}{2}, \frac{a}{2(1+2c)})$, which are proportional to a. It makes sense that when a is very small, $\omega_+ \approx \omega_-$ and $\nu_+ \approx \nu_-$; when a approaches zero, we recover the solutions (8) of the non-dissipative case.

13

(ii) $a = 2$:

$$\varphi(t) = e^{-t}t + \frac{1+2c}{\sqrt{2c}}e^{-\frac{1}{1+2c}t}\sin\left(\frac{\sqrt{2c}}{1+2c}t\right) \tag{19a}$$

$$\theta(t) = e^{-t}t - \frac{1+2c}{\sqrt{2c}}e^{-\frac{1}{1+2c}t}\sin\left(\frac{\sqrt{2c}}{1+2c}t\right) \tag{19b}$$

(iii) $2 < a < 2\sqrt{1+2c}$ (medium dissipation):

$$\varphi(t) = \frac{2}{\sqrt{a^2-4}}e^{-\frac{a}{2}t}\sinh\left(\frac{\sqrt{a^2-4}}{2}t\right) + \frac{2}{\sqrt{4\beta-\alpha^2}}e^{-\frac{\alpha}{2}t}\sin\left(\frac{\sqrt{4\beta-\alpha^2}}{2}t\right) \tag{20a}$$

$$\theta(t) = \frac{2}{\sqrt{a^2-4}}e^{-\frac{a}{2}t}\sinh\left(\frac{\sqrt{a^2-4}}{2}t\right) - \frac{2}{\sqrt{4\beta-\alpha^2}}e^{-\frac{\alpha}{2}t}\sin\left(\frac{\sqrt{4\beta-\alpha^2}}{2}t\right) \tag{20b}$$

where $\alpha = \frac{a}{1+2c}$ and $\beta = \frac{1}{1+2c}$.

(iv) $a = 2\sqrt{1+2c}$:

$$\varphi(t) = \frac{1}{\sqrt{2c}}e^{-\sqrt{1+2c}t}\sinh\left(\sqrt{2c}t\right) + e^{-\frac{1}{\sqrt{1+2c}}t}t \tag{21a}$$

$$\theta(t) = \frac{1}{\sqrt{2c}}e^{-\sqrt{1+2c}t}\sinh\left(\sqrt{2c}t\right) - e^{-\frac{1}{\sqrt{1+2c}}t}t \tag{21b}$$

(v) $a > 2\sqrt{1+2c}$ (large dissipation):

$$\varphi(t) = \frac{2}{\sqrt{a^2-4}}e^{-\frac{a}{2}t}\sinh\left(\frac{\sqrt{a^2-4}}{2}t\right) + \frac{2}{\sqrt{\alpha^2-4\beta}}e^{-\frac{\alpha}{2}t}\sinh\left(\frac{\sqrt{\alpha^2-4\beta}}{2}t\right) \tag{22a}$$

$$\theta(t) = \frac{2}{\sqrt{a^2-4}}e^{-\frac{a}{2}t}\sinh\left(\frac{\sqrt{a^2-4}}{2}t\right) - \frac{2}{\sqrt{\alpha^2-4\beta}}e^{-\frac{\alpha}{2}t}\sinh\left(\frac{\sqrt{\alpha^2-4\beta}}{2}t\right) \tag{22b}$$

where $\alpha = \frac{a}{1+2c}$ and $\beta = \frac{1}{1+2c}$.

As an example, for the above categories we set (i) $a = 2\sqrt{1-c}$, (ii) $a = 2$, (iii) $a = 2\sqrt{1+c}$, (iv) $a = 2\sqrt{1+2c}$ and (v) $a = 2\sqrt{1+3c}$ (for $0 < c < 1$). The solutions are shown in fig.8 with $c = 0.1, 0.5$ and 0.9, respectively.
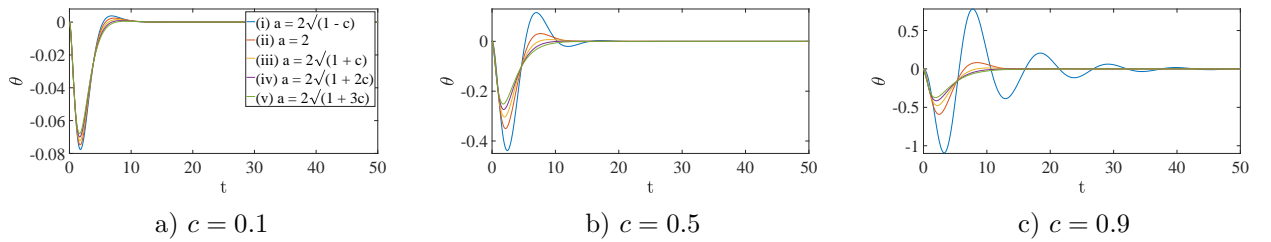

a) $c = 0.1$ b) $c = 0.5$ c) $c = 0.9$

Figure 8: Examples of axion solution curves ($t_{max} = 50$) in the case of dissipation.

14

6. The effect of an external magnetic field

Coupled Josephson junctions, when treated quantum mechanically, can form SQUIDs (superconducting quantum interference devices), which are very sensitive to small magnetic fields. Moreover, axions also have non-trivial interactions with magnetic fields, for example they can decay in strong magnetic fields into two photons. It has also been suggested that magnetic flux noise phenomena in coupled q-bits and SQUIDs can yield valuable information about axion physics [23]. It is thus interesting to study the effects of weak and strong magnetic fields for our coupled (classical) axion-Josephson system.

To take into account magnetic fields, our system dynamics is extended to

$$\ddot{\varphi} + a_1\dot{\varphi} + b_1\sin\varphi = c(\ddot{\theta} - \ddot{\varphi}) + d_1(\varphi + e_1) \tag{23a}$$

$$\ddot{\theta} + a_2\dot{\theta} + b_2\sin\theta = c(\ddot{\varphi} - \ddot{\theta}) \tag{23b}$$

where $d_1 = -\Phi_0/2\pi L I_c$ is a material constant and $e_1 = 2\pi\Phi/\Phi_0$ is the normalised applied flux (with Φ_0 the flux quantum, L the inductance, I_c the critical current, and $\Phi = |\vec{B}| \times Area$), the external magnetic field is $\vec{B}$, cf. [9]). Referring to experiments described in [19], we choose $a_1 = a_2 = 5 \times 10^{-5}, b_1 = b_2 = 1, c = 2.31 \times 10^{-3}, d_1 = -0.352$ and allow e_1, which is determined by the strength of the external magnetic field, to vary from 0 to 100. Note that unlike the model in [19], the second equation in the above system describes the axion dynamics and there is no *a priori* reason to include a similar flux term as in the first equation. For our numerical simulations in the following, the initial conditions are chosen in the same way as in section 2.

The phase space structure for this full system is more complicated than in the previous cases: an interesting phenomenon occurs when e_1 increases from $\frac{\pi}{2}$ via π to $\frac{3\pi}{2}$, see fig.9 below.
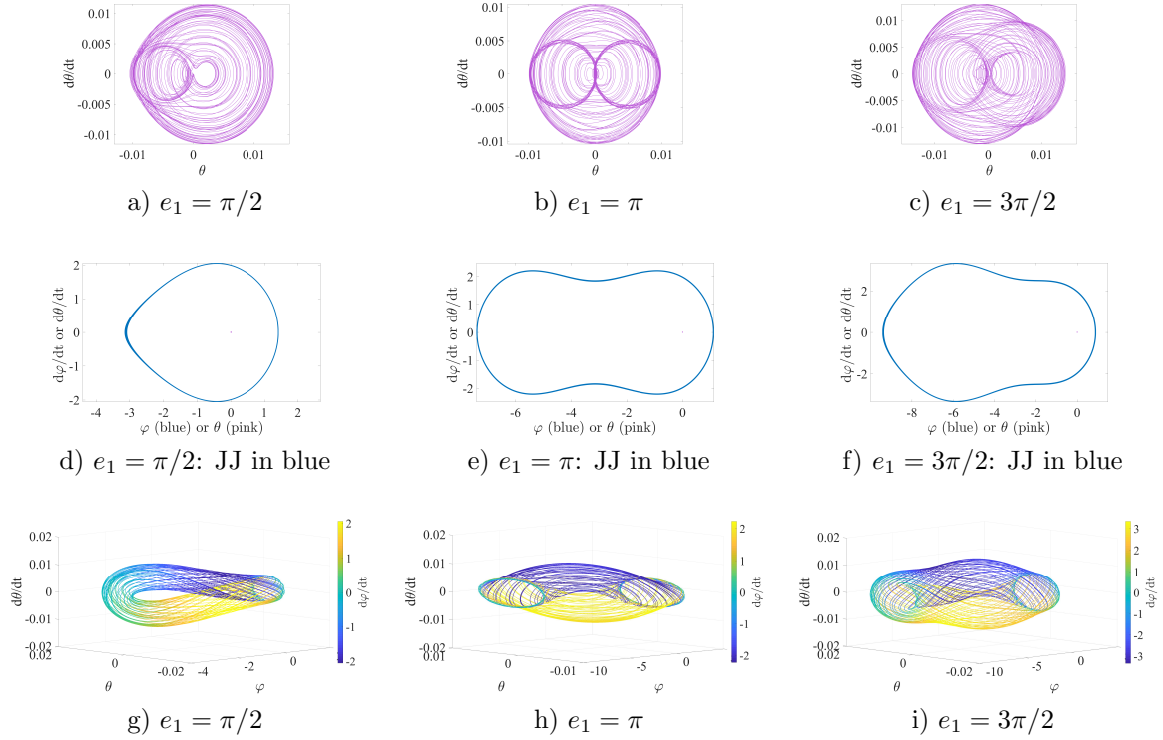
Figure 9: Effect of an external magnetic field with $e_1 = \pi/2, \pi, 3\pi/2$: first row: axion phase trajectories; second row: the corresponding trajectories for both Josephson junction (JJ) and axion (in each plot the almost invisible pink dot at the origin represents the relative size of the axion oscillation); last row: the corresponding $(\varphi, \theta, \dot\theta)$-subspace with color coding representing the value of $\dot\varphi$ ($t_{max} = 500$)

Comparing the phase portrait structure near the transition point at $e_1 = \pi$, we observe an interesting topological phase transition: The cyan side of fig.9g is everted to make the whole structure being twisted on both ends — the dark blue and light yellow bands cross each other twice (like an inside-out torus), and the cyan parts become two thin circles which correspond to the '∞' that appears in the axion phase trajectory (fig.9b). The overall topological deformation undergoes a procedure like a torus eversion: from a torus (for $e_1 \sim 0$) to a one-side everted torus (for $e_1 \sim \frac{\pi}{2}$) to a two-side everted torus (for $e_1 \sim \pi$) to finally an inside-out torus (for $e_1 \sim \frac{3\pi}{2}$). This complicated topological phase transition illustrates that the effect of small magnetic fields for coupled Josephson systems is profound, and occurs already in the classical treatment. For a large enough magnetic field $e_1 \sim 100$ the phase portrait of the Josephson junction (in blue) approaches an ellipse while the two bands in the subspace are densely interwoven and eventually fill the whole structure in phase space.

7. Conclusion

The classical dynamics of coupled axion-Josephson junction dynamical systems exhibits a surprisingly large complexity which we have investigated in detail in this paper. When changing either the coupling constant or the initial angular velocity, we observed eversion

processes where a simple cardioid-shaped trajectory splits into multiple copies, with a different topology above and below the eversion point. Close to resonance points, where the plasma frequency of the junction coincides with the axion mass ($b_1 = b_2$), there is extreme sensitivity of the structure of the phase portrait depending on the ratio of Josephson to axion frequency. In the limit of small elongations, we proved that for certain distinguished coupling constants the coupled system generates time-shifted identical trajectories for the axion and the Josephson junction, however these oscillations have much richer structure and the phase portrait depends in a complicated way on two integers k, k_1 that make up the coupling constant $c = \frac{2k^2}{(2k_1+1)^2} - \frac{1}{2}$. From a physical point of view this result is very interesting, because it shows that even in the limit of extremely small coupling $c \to 0$ the axion and Jospsephson junction trajectory can synchronize in a time-shifted way, meaning that the (measured) Josephson junction phase angle mirrors the behavior of the axion. The introduction of a magnetic field makes the phase portrait even more complex, with topological transitions and torus eversions at critical values of the magnetic field. Our investigation was motivated by the need to understand the dynamics (and possible signals) in future axion detectors based on Josephson junctions or coupled Josephson junctions, which have been suggested in the recent literature [9, 10, 11, 12]. For realistic detector scenarios one would need to proceed from a classsical description to a quantum description, which is out of the scope of the current paper. However, interestingly enough already the classical dynamics is extremely complex, and this will imprint onto the quantum dynamics.

References

[1] R.D. Peccei, H. Quinn, Phys. Rev. Lett. 38, 1440 (1977)

[2] F. Wilczek, Phys. Rev. Lett. 40, 279 (1978)

[3] S. Weinberg, Phys. Rev. Lett. 40, 223 (1978)

[4] B.M. Roberts, Y.V. Stadnik, V.A. Dzuba, V.V. Flambaum, N. Leefer, D. Budker, Phys. Rev. Lett. 113, 081601 (2014)

[5] P.W. Graham, S. Rajendran, Phys. Rev. D 88, 035023 (2013)

[6] P. Sikivie, Q. Yang, Phys. Rev. Lett. 103, 111301 (2009)

[7] L. Visinelli, P. Gondolo, Phys. Rev. Lett. 113, 011802 (2014)

[8] M.P. Hertzberg, M. Tegmark, F. Wilczek, Phys. Rev. D 78, 083507 (2008)

[9] C. Beck, Mod. Phys. Lett. A 26, 2841 (2011)

[10] C. Beck, Phys. Rev. Lett. 111, 231801 (2013)

[11] C. Beck, Phys. Dark Univ. 7-8, 6 (2015)

[12] C. Beck, Proc. of Science EPS-HEP2017 058 (2017) [arXiv:1710.04299]

[13] M. Tinkham, *Introduction to Superconductivity*, Dover Publ., New York (2004)

[14] D. G. Aronson, arXiv: 1707.00038

[15] T.Hongray, J. Balakrishnan, S. K. Dana, Chaos 25, 123104 (2015)

[16] C. Bick, P. Ashwin, A. Rodrigues, Chaos 26, 094814 (2016)

[17] T. P. Valkering, C. L. A. Hooijer, M. F. Kroon, Physica D 135, 137 (2000)

[18] M. Steffen et al., Science 313, 1423 (2006)

[19] J.A. Blackburn, J.E. Marchese, M. Cirillo, N. Groenbech-Jensen, Phys. Rev. B 79, 054516 (2009)

[20] B.T. McAllister et al., Phys. Dark Univ. 18, 67 (2017)

[21] C.A.J. O'Hare, A.M. Green, Phys. Rev. D 95, 063017 (2017)

[22] J.W. Foster, N.L. Rodd, B.R. Safdi, Phys. Rev. D 97, 123006 (2018)

[23] C. Beck, Scientific Rep. 6, 28275 (2016)